Mild Hybrid Multi-Energy Systems: Waste Energy Recovery by Bottom ORC System

Roberto Capata

Sapienza, University of Roma

Abstract:

The goal of this paper is to evaluate, from a thermodynamic point of view first, and then constructive one, the possibility of inserting a waste heat recovery system in a hybrid vehicle in mild-hybrid configuration. The vehicle considered is a standard 1000 cc gasoline turbocharged ICE. The characteristic and proposed configuration of the vehicle allows to mechanically separate the existing turbo-compressor unit and to couple them with the respective electrical devices: electric motor and generator. This new architecture enables an electrical generation that can be used to recharge the installed battery package. Moreover, thanks to the new configuration of the turbine of the group, i.e. without the wastegate valve, the turbomachinery provides a high gas flow rate at high temperature (about 380 °C). These exhaust gases can be used for a bottom ORC group, with additional electricity generation. All these considerations permit to have an extra on-board recharge of the batteries, to consequently increase the electric range of the vehicle (a sort of range extender) and to install a battery group of limited size and power, with consequent advantages of payload and vehicle efficiency. Besides, it allows to achieve the well know and inflated aspects (from a citation point of view) of the emissions reduction.

Keywords:

Mild Hybrid Vehicle, Electric Generation, ORC plant, Compressor Turbine Condenser design

1. Introduction

The aim of the research is to verify the feasibility of an on-the-road prototype of a power train for a hybrid propulsion vehicle. In detail, the project consists in the study and implementation of an innovative complex energy plant for the ICE (900cc) of a city car [1-4]. The solution studied is to mechanically disconnect the compressor/turbine complex, supporting the C compressor with a dedicated electric motor and connecting the T turbine to a generator. Mechanical C/T decoupling allows both machines to be designed so that they operate close to the maximum efficiency point for the maximum part of the expected real operating range. Specifically, the turbine has a lower rotation speed than that of the original group and therefore is characterized by slightly larger dimensions. The advantage is that in current supercharger units the surplus at high revs is discharged through the waste-gate valve without expanding into the turbine. In the configuration proposed here, however, all the energy of the gases is used by the turbine to generate electrical power, that can be used where required. Finally, with a view to optimizing all energy flows, the turbine exhaust is used for a bottoming ORC group, for electricity generation. The surplus of energy thus obtained can be used to power the auxiliaries, reducing both fuel consumption and lengthening the time of use of the electrical part, via battery pack. The actions taken were [5]:

a) Study a suitable configuration of a new turbocharging unit (hereinafter, "TC") for the specific thermal engine chosen here (ICE 900 cc turbo ≈ 66 kW), separating the compressor and the turbine and realizing the two devices with ad hoc components;
b) Simulate the behavior of the new TC group over the entire operating range of the engine, possibly making appropriate changes to the configuration originally chosen;
c) Design and implement a prototype configuration of the new C/T group (integrating the part relating to the motorization/electric generation and test it in advance);
d) Simulate and design the submitted ORC group.

2. Compressor and Turbine design

Once the engine of the vehicle (999 cc) of the city car being searched was established, the existing group on the vehicle was identified, the operational map of which is shown in figure 2.

https://doi.org/10.52202/069564-0244

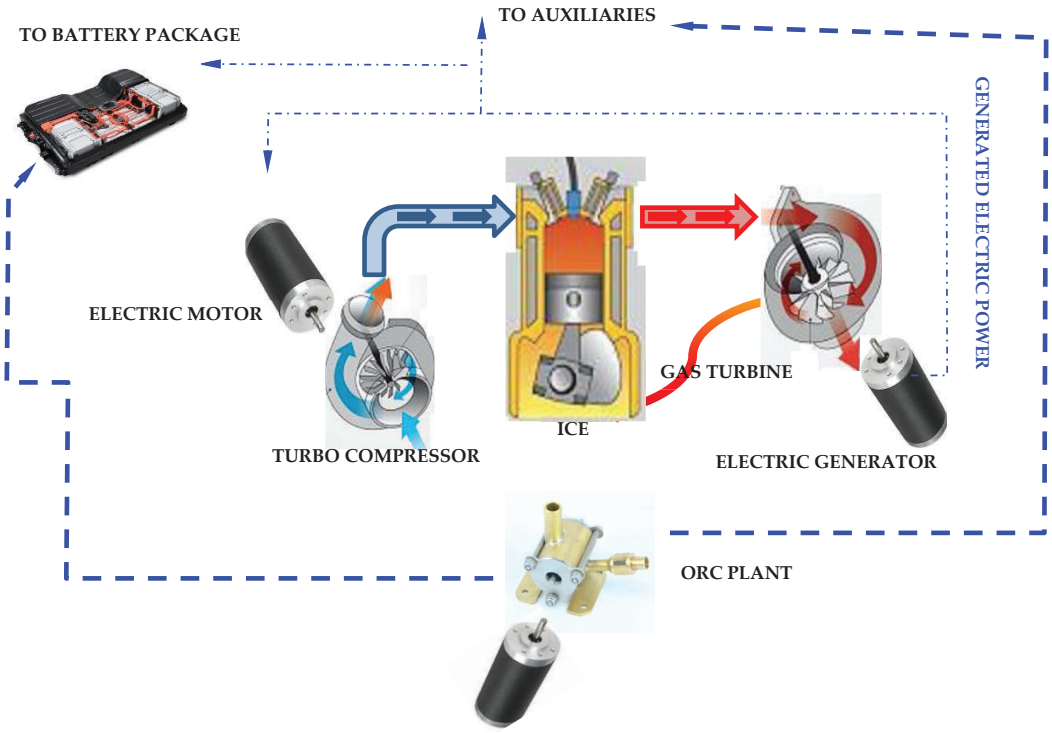

Figure 1. The electro-assisted configuration of the proposed turbocharging unit and the ORC group

Based on the n_s/d_s design theory [5-8], the geometric characteristics of the compressor shown in table 1 are obtained. Obviously, the dimensions and speeds are established here based on the values provided by the manufacturer of the installed compressor. The operating point was also fixed and derived since the maps of the business model [5,6]. The operating specifications are as follows:

$\beta = 1.5$
$\dot{m} = 0.02\text{-}0.06$ kg/s
n = 140000-210000 rpm

the range includes operation at the minimum and maximum speeds assumed by the ICE (2000-5000 rpm)

Table 1. Compressor data designed

m [kg/s]	0.02	**W_{EUL} [J/kg K]**	44652.74	**ψ_2**	1
β	1.4	**U_2 [m/s]**	211.3	**ψ_1**	0
c_p [J/kg K]	1004	**r_2 [m]**	0.014421	**φ_1**	0.3
T_1 [K]	293	**ΔT [K]**	22	**φ_2**	0.55
ω [rad/s]	14653	**ρ_1 [kg/m^3]**	1.20108	**δ_p**	0.98
ε	0.42	**Q_1 [m^3/s]**	0.016652	**χ**	0.65
p_1 [Pa]	101000	**r_{1e} [m]**	0.011005	**R_p**	0.5
T_2 [K]	337	**r_{1i} [m]**	0.007153	**$(1-\chi^2)$**	0.5775

From the analysis of the data it can be noticed the correspondence to the existing model, installed in the vehicle. The operation of the compressor at various speeds of the ICE engine was then evaluated and using the previous map it was possible to fill in the following table and the figure shows the trend of the power required by the compressor as the number of revolutions of the ICE changes.

Table 2. Compressor operation at different ICE speeds

rpm ICE	$\dot{m}$ [kg/s]	rpm	β_c	T_{in} [K]	T_{out} [K]	P [W]	η
2000	0.021	145000	1.42	298.4	344	920.71	0.68
3500	0.0408	180000	1.64	297.5	354	2474.39	0.8
5500	0.0619	210000	1.84	297.5	366.8	4444.96	0.82

https://doi.org/10.52202/069564-0244

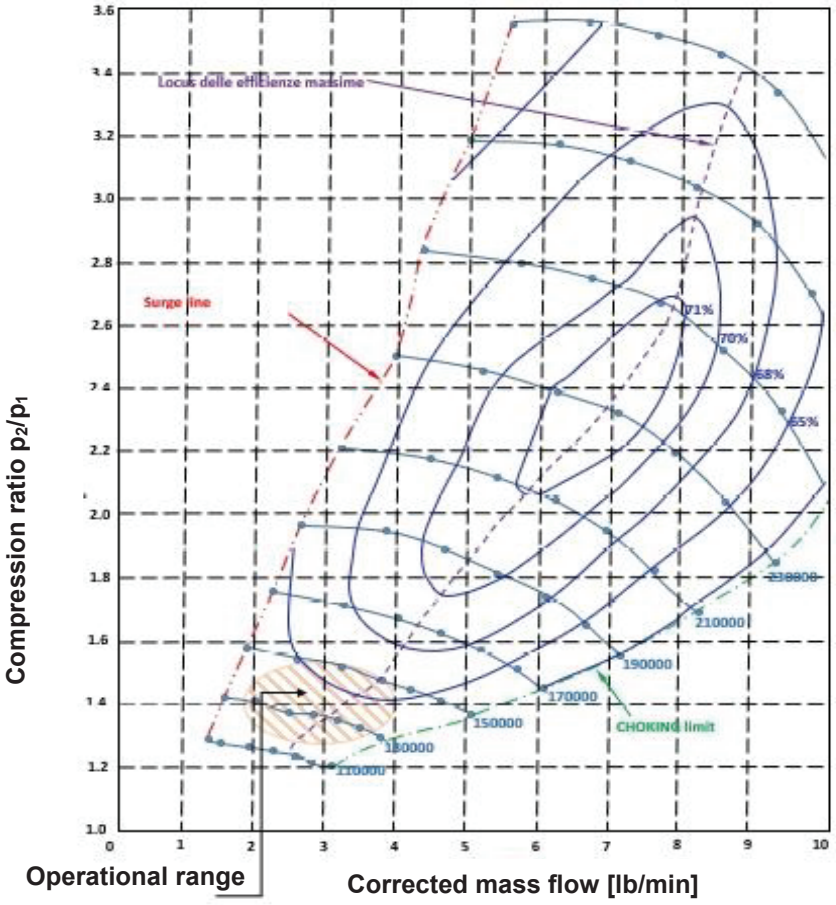

Figure 2. Compressor chart

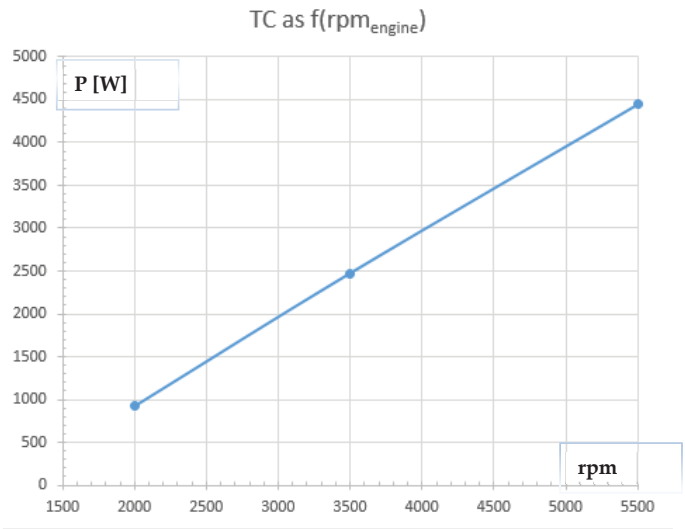

Figure 3. Compressor power required as a function of the ICE speed

Using the same procedure described above, the turbine was designed [9-15]. The main characteristics are shown in Table 3.

https://doi.org/10.52202/069564-0244

Table 3. Turbine data

m [kg/s]	0.021	**L_{EUL} [J/kg K]**	103194	ψ_2	0
β	1.4	**U_2 [m/s]**	321.2	ψ_1	1
c_p [J/kg K]	1397	**r_2 [m]**	0.051153	φ_1	0.3
T_1 [K]	980	**ΔT [K]**	34	φ_2	0.4
ω [rad/s]	6280	**ρ_2 [kg/m^3]**	0.387992	δ_p	0.98
ε	0.23	**Q_2 [m^3/s]**	0.05412	χ	0.65
p_2 [Pa]	101000	**r_{1e} [m]**	0.011159	**R_p**	0.5
T_2 [K]	907	**r_{1i} [m]**	0.007253	**$(1-\chi^2)$**	0.5775

From the analysis of the data, the correspondence to a turbine model available on the market is evident, whose operational map is represented in figure 4. The operation of the turbine at various ICE engine speeds was then evaluated using the map, so the turbine trend generation is reported in figure 5 and, as above, it is possible to fill the following table, in function of ICE speed.

Table 4. Turbine operation at different ICE speeds

rpm ICE	$\dot{m}$ [kg/s]	rpm	β_c	T_{in} [K]	T_{out} [K]	P [W]	η
2000	0.024	82170	1.2	954	922	780	0.87
3500	0.04	134483	1.6	1005	930	3510	0.86
5500	0.07	164002	2.00	1045	932	9500	0.81

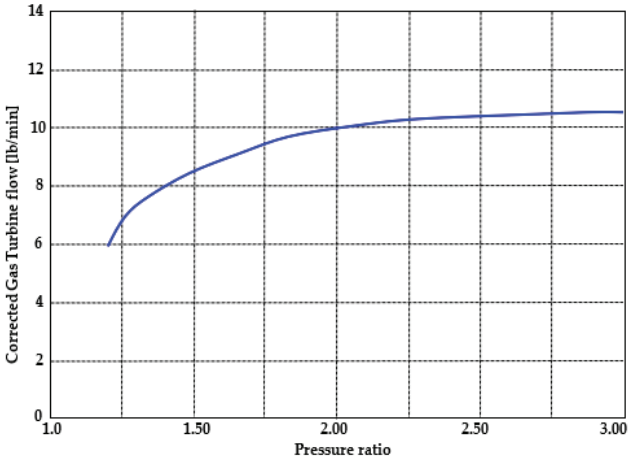

Figure 4. Turbine operational chart

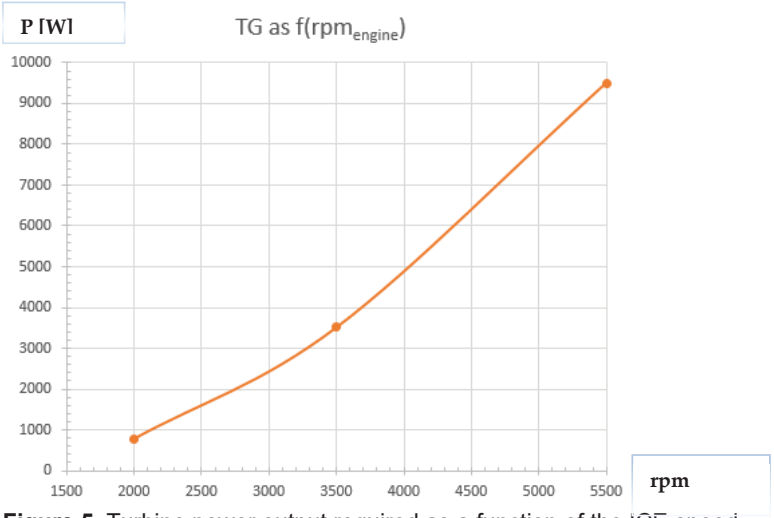

Figure 5. Turbine power output required as a function of the ICE speed

https://doi.org/10.52202/069564-0244

3. Energy Recovery and Vehicle Energy Balance

Thanks to the proposed design changes, the new electrically assisted turbocharger offers extra power at all engine speeds, except for about 2500 rpm and the power curve are shown in figure 6. It can be noted that the reported values include mechanical and electrical efficiency. For any type of mission (ETC, EUDC, WVU and NDC [17-21]), the engine energy balance is calculated by calculating the instantaneous power demand to the wheels, adding transmission losses, adding the compressor power and subtracting it from the turbine power and considering the battery charging efficiency. The effect of KERS has not been included in the simulations at this time. For almost the entire mission, the turbocharger unit can deliver extra net power. This power will be used mainly to recharge the battery pack and power the auxiliaries. When the power is negative (almost always on restart and during braking operations) the compressor will draw the required power from the on-board battery package. Since the vehicle is conceived as a *mild hybrid*, this battery pack is obviously much smaller than in a common HEV [22-29]. In longer missions, the instantaneous surplus generated by the turbocharger, minus the contributions sent to the auxiliaries, can lead to a condition in which the battery pack has a SOC close to 100% and cannot accept further charges. In these circumstances, the extra power could be used or sent to an auxiliary electric motor for additional propulsion.

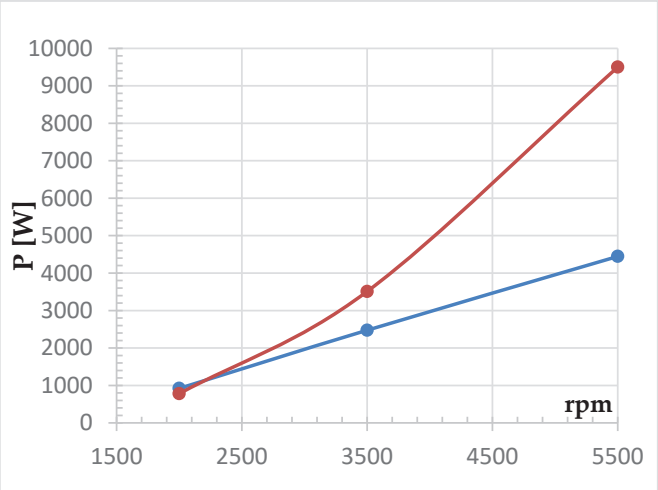

Figure 6. Power of the Turbine (orange curve) and the Compressor (blue) as a function of ICE rpm

The proposed solution, namely to physically decouple the compressor and turbine, using an electric motor for the first and producing electricity from the second via electric generator, showed that the total energy recovered on the simulated missions amounts to 1.01 kWh (compared to the 18 kWh of total energy required by the vehicle), which means that a net saving of about 5.6% can be achieved by the installation of this new turbocharger unit (figure 7).

4. The Bottoming ORC cycle

A further optimization of the considered system is to insert a bottoming ORC cycle. This possibility is thermodynamically feasible because the outlet temperature of the exhaust gases from the turbine, which must be remembered that it works without a wastegate valve, is about 800 K. The fluid used is an organic fluid R245fa. In the worst case, the exhaust gas flow rate is 0.024 kg/s. This temperature is high for a typical ORC application, especially for the required low power; this means that the energy content is too high and probably the use of Rankine Cycle instead an ORC would be more efficient, nevertheless for a compact application an organic fluid is more convenient, because the dimensions of the heat exchangers are smaller. Using commercial software, the thermodynamic simulation of the ORC cycle was performed. Among the various parameters to be set, the value of the maximum power that can be delivered, of about 2 kW, was chosen. Since the power is not high, it is not convenient to design a sophisticated cycle with preheaters or re-heaters commonly used in large-size plant. Thus, the cycle is very simple and only few components are required (Fig. 8) [30-35]:

1. Air Heat Recovery: it is a heat exchanger where the organic fluid warms up and changes its phase from liquid to vapor. This transformation is considered isobaric and, in the phase, changing is also isothermal.

https://doi.org/10.52202/069564-0244

2. Expander: it operates between the pressure imposed upstream and downstream by the heat recovery and the condenser.
3. Condenser: used to condensate the organic fluid with water. This transformation is considered isobaric and isothermal during the phase changing.
4. Pump: it increases the pressure of the organic fluid, now liquid, up to the pressure inside the Air Heat Recovery.
5. Flow Mixer: necessary to add the possible make up flow rate.

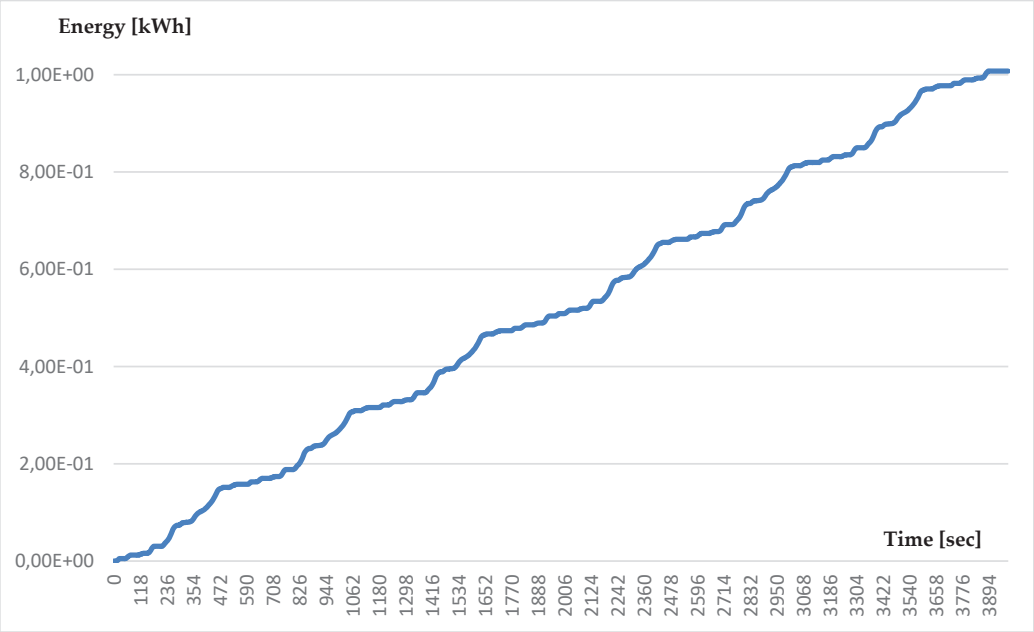

Figure 7. Net energy supplied by the GT group during the mission

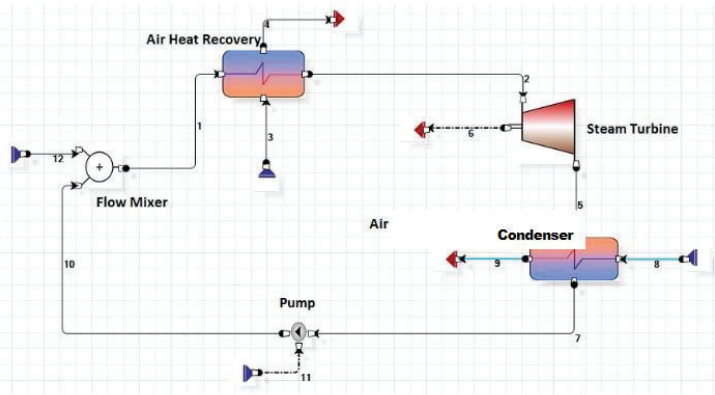

Figure 8. ORC cycle layout

From the statement of the problem, the input constrains are:

- The output power from the turbine (flow 6): 2 kW
- The available mass flow rate of the exhaust gas (flows 3): 0,024 m^3/s
- Temperature of the exhaust gas (flows 3): 723 K (conservative set)

https://doi.org/10.52202/069564-0244

The temperature of the inlet water is set to 293 K, hence, considering the finite dimensions of the condenser and its losses, the organic fluid should condense at 301 K, because it cannot reach lower temperature. Thanks to the thermodynamics properties, setting the condensation temperature means that the condensation pressure is fixed. From the thermodynamics tables for R245fa, this fluid condenses at 301 K with a pressure of 170 kPa. The expander efficiency has been underrated at 0.7 to be sure that the outlet power was at least 2 kW and the efficiency of the pump is fixed to 0,9. The results obtained by the process simulation indicates a mass flow rate for the organic fluid of 0.13 kg/s.
In summary, thermodynamic feasibility of whole system is confirmed. The current state of research focuses on the advisability of using a helical evaporator [36] for the ORC plant. For the study of the expander we will follow the procedure described in previous papers [31-37], trying to define the more efficient device. Only the condenser is under evaluation. First, the possibility of using the existing radiator of the car has been considered, but due to the limited overall available dimensions a compact capacitor [38-42] is being studied.

Table 5. R245fa operating specifications

Mass flow rate [kg/s]	0.13
Evaporator inlet temperature [K]	301
Evaporator outlet temperature [K]	383
Condenser inlet temperature [K]	370
Condenser outlet temperature [K]	301
Condenser inlet pressure [Pa]	170000
Water inlet temperature [K]	293
Water outlet temperature [K]	301
Pump required power [W]	100
Power output [W]	2000

4.1. Condenser design procedure

The chosen configuration (Figure 9) is the “circular tube fin”. It has several advantages such as reduced weight, better temperature control and easier transport. The type of tube is often chosen to reduce losses [28,29]. The inner diameter of the tube is 8 mm, the fin length is 3 mm, the tube thickness is 1 mm and the distance between two consecutive fins is 2 mm. The staggered arrangement is triangular, to avoid interference problems, and the distance between each arrangement center is 17 mm (the distance will be called p_t or p_l if it is from tube to tube or from tube to the outer shell). After the number of tubes is set, the width, thickness, and length are defined. At this point, we must distinguish what happens in the mono-phase or the two-phase condensation. The analysis will be conducted for both the working fluid (inside) and the water (outside).

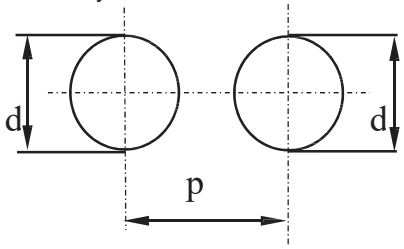

Figure 9. Reference scheme.

4.1.1 Monophasic Condensation

Working fluid side

The fluid characteristics (viscosity coefficient, thermal conductivity, etc.), were derived from the Coolprop library. First, the enthalpy difference is calculated to compute the thermal exchange. Then, the LMTD is derived with the HEM method. It is now necessary to compute the overall heat coefficient U to find the required exchange area. To compute the coefficient U we have to introduce the basic dimensionless numbers: Reynolds, Nusselt, Prandtl, and Froude. Once all quantities have been defined, the following procedure will be used.

1. The Prandtl number is calculated, and secondly, the calculation of the fluid velocity inside the pipes is evaluated, permitting the evaluation of the Reynolds number, which leads to the Nusselt numbers.

https://doi.org/10.52202/069564-0244

2. After computing the Nusselt numbers, it is then possible to estimate the "h_i" that is the heat transfer coefficient.
3. Finally, it is necessary to introduce the areas. When the numbers of tubes are known, where N_s is the number of pipes where the mass flow condensate, N_r is the numbers of transits of the same bundle of tubes, and the total number N_t, the geometrical properties can be calculated. The inner area of the pipes is:

$$A_i = \pi d_i \, L_1 \, N_t \quad (1)$$

and the minimum free flow area is:

$$A_{0,i} = \frac{1}{4}\pi \, d_i \, N_s \quad (2)$$

Cooling fluid side

As previously mentioned, the characteristics of the fluids are derived from the Cool- prop library. The main areas (external pipes side) are the A_p, the primary area, the fin area A_f and the heat transfer surface area A_0. The primary area is the difference between the pipe surface area and the area blocked by the fins. The A_0 is the total heat transfer area, computed by the sum of the primary area and the fin area. Another important parameter to determine is the minimum areas among the pipelines, where the water flows. If a triangular configuration is chosen [29], it is possible to consider that surface, as a flat surface.

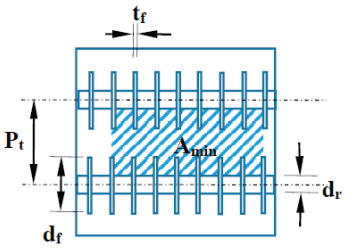

Figure 10. Minimum area description of the condenser.

4.2. Biphasic Condensation

As the condensation process proceeds along the pipes, the working fluid velocity decreases. At first, the condensation will occur on the wall of the pipes, then layer by layer, the liquid phase will increase. When the fluid is condensing, its thermodynamic characteristics change. The same procedure for the mono-phase has been adopted, introducing some necessary changes [40-44]. The evolution of the working fluid, from quality "0" to quality "1", has been divided into four-parts.

1. Part one, when the quality x is within 0 ÷ 0.75.
2. Part two, when x = 0.75 ÷ 0.5.
3. Part three, when x = 0.5 ÷ 0.25.
4. Part four, when x = 0.25 ÷ 0.

Similarly, for the cooling fluid side, there will be four corresponding stages. The four stages of the cooling water have been computed, if every property is changing linearly. From the working fluid side, the Martinelli parameter is introduced to compute the Nusselt number. The formulae used for the R245fa is:

$$Nu = 0.023 Re^{0.8} \, Pr^{0.3} \, g(Xtt) \quad (3)$$

4.2 Design results

The system geometry has been defined respecting the required constraints. A square configuration of the condenser has been chosen. The previous Figure 10 represents the simulated condenser. Streams numbers 1 and 2 are the inlet and outlet of the working fluid, and streams 4 and 5 are the inlet and outlet of the cooling fluid. Stream 3 is the refill of the fluid; in this case, it is not considered, but it is important to mention the fact that this opportunity exists. Table 6 reports the operating specifications of the main streams. After numerous iterations, the optimal solution has been found. The considered configuration is a compromise between a reasonable pressure drop and the smallest area. All data and a representation of the condenser are, respectively, reported in Table 7 and Figure 11

https://doi.org/10.52202/069564-0244

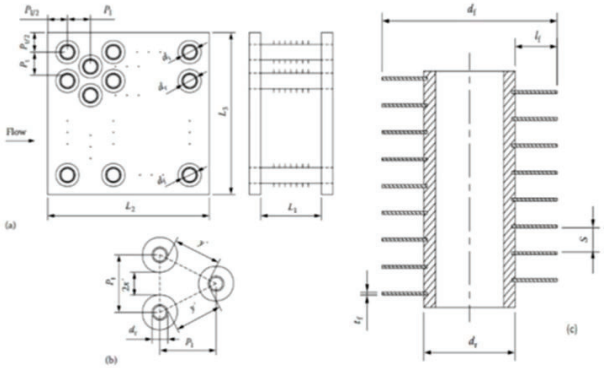

Figure 11. The condenser's chosen configuration. (a) actual disposition in the condenser assembling, (b) triangular configuration characteristics, (c) finned pipe representation.

Table 6. Condenser Streams.

Stream n° 1	
Temperature (K)	383
Pressure (kPa)	610
Stream n° 2	
Temperature (K)	346
Pressure (kPa)	606
Stream n° 3	
Temperature (K)	332
Pressure (kPa)	101.3
Stream n° 4	
Temperature (K)	301.2
Pressure (kPa)	170.3

Table 7. The condenser's main dimensions.

L_1	0.22
L_2	0.22
L_3	0.18
d_i	0.007
d_r	0.01
d_f	0.014
P_t	0.016
P_l	0.016
S (m)	0.002
t_f (m)	0.0003
N_r	16
N_s	14
N_{tot}	16 × 14 = 224

https://doi.org/10.52202/069564-0244

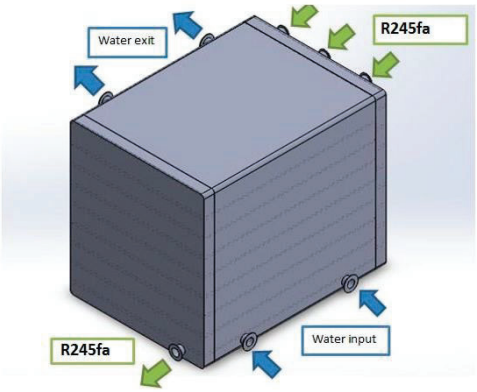

Figure 12. Condenser 3D assembled view.

Finally, the procedure adopted for the design is satisfactory. In fact, given that one of the constraints is the limited space inside the vehicle (the design philosophy is, remember, not to modify the vehicle and to use, when this is possible, all the existing devices and components), the exchanger obtained is small and can be easily inserted inside the vehicle, as will be described in the following paragraph.

5. The On-Board configuration of ORC cycle

An empirical method has been used to demonstrate that the proposed ORC system can be mounted on a vehicle. In the considered commercial vehicle, respecting the available spaces and volumes, the tank has been replaced and modified. For the positioning in the vehicle, since the HRSG has not been measured (at present), it has been assumed to be the same size as the condenser. It is known that the HRSG device is usually smaller than the condenser. Figures 13 represent the possible plant configuration in a commercial vehicle. It is important to remember that it is necessary to realize an auxiliary circuit forthe water cooling.

Figure 13. Proposed on-board ORC assembled plant configuration view.

Future Developments and Conclusions

The next steps in the realization of the vehicle and therefore for the completion of the project, the electrical part is now testing. The compressor side tests have almost been completed and have given satisfactory results and in line with what was assumed and chosen. On the turbine side, the test bench has been assembled, which involves the use of a rechargeable battery of about 17 kWh, and once the electrical connections have been completed, will be tested.

At the same time, the expander and evaporator for the ORC group will be designed, always trying to respect the overall constraints imposed by the chosen vehicle. As far as the expander is concerned, we will opt for a

https://doi.org/10.52202/069564-0244

compact solution and consequently the choice could fall on a dynamic expander or most likely on a rotary volumetric, screw type. For the evaporator, the opportunity to create a helical heat exchanger coaxial to the turbine exhaust pipe is being studied, to reduce the size as much as possible.
In conclusion, a very important and “innovative” aspect was the possibility of creating, as part of the electrification process of the power train for the mild hybrid, a “direct coupling” between the electric motor and compressor, and to optimize all waste energy fluxes of the vehicle. All these are thanks to the design of a new electric motor, operating at high rotational speeds, which are characteristics of turbomachinery. The redesigned turbine (now separated from the compressor) has confirmed to be less problematic than the compressor. The turbine can now use all the enthalpy drop of the ICE exhaust gases and operate at lower speeds. As a result, the connected electrical equipment is less complicated, compared to that designed and built for the compressor. The tests - cold site - validate the design choices and the further turbine ones - in case of positive results - confirm and "freeze" the electrical configuration. Then, thanks to the characteristic configuration of the turbine (no wastegate valve), the total exhaust gases can be used for generate additional energy by ORC plant. The bottoming ORC systems has to be completed, from a design point of view. Actually, the condenser realization is "on going". Once realized, a "substitute" circuit will be realized to simulate the operational conditions. The simultaneously design of expander and evaporator will conclude the design process. Last step will be to implement all devices and test the vehicle on the road.

Nomenclature

C	Compressor
EM	Electric Motor
EG	Electric Generator
ICE	Internal Combustion Engine
m	Mass flow rate [kg/s]
p	Pressure [bar]
P	Power [W], Pump, Pressure gauge
Q	Volumetric flow rate [m^3/s]
r	Radius [m], Resistance [Ω]
rpm	Revolutions per minute
R_ρ	Reaction degree
T	Temperature [K], Turbine
V	Velocity
Greek Symbol	
β	Compression ratio
χ	Hub to shroud ratio
δ	Blockage factor
ϵ	Diameter ratio
η	Efficiency
ϵ	Flow coefficient
ω	Rotational speed Density
ρ	[kg/m^3]
ψ	Load coefficient

References

[1] Yu H.; Song K.; Xie H. Research on Optimal Control of Air System of Diesel Engine with ETurbo Based on Model Prediction. *Chin. Intern. Combust. Engine Eng.* **2018**, *3*, 39–46.

[2] Song K.; Xie H.; Upadhyay D. An assessment of performance trade-offs in diesel engines equipped with regenerative electrically assisted turbochargers. *Int. J. Engine Res.* **2018**, 1–17.

[3] Dimitriou P.; Burke R.; Zhang Q.; Copeland C.; Stoffels H. Electric turbocharging for energy regeneration and increased efficiency at real driving conditions. *Appl. Sci.* **2017**, *7*, 350.

[4] Capata R. Urban and extra-urban hybrid vehicles: A technological review. *Energies* 2018 (11), 2924; https:// doi.org/10.3390/en11112924

[5] Capata R., Sciubba E. Preliminary Analysis of a New Power Train Concept for a City Hybrid Vehicle. *Designs* 2021, 5(1), 19; https://doi.org/10.3390/designs5010019

[6] Capata R. Experimental Fitting of Redesign Electrified Turbocompressor of a Novel Mild Hybrid Power Train for a City Car. *Energies* 2021, 14(20), 6516; https://doi.org/10.3390/en14206516

[7] Shepherd J. Principles of Turbomachinery. J. Macmillan Pub. Co, NY 1956.

[8] Balje O. Turbomachines". Wiley & Sons, 1981.

[9] ATIP Scoop, Japan Office, "*Micro Gas Turbine Development*", Feb 2005.

[10] Capata R., Sciubba E. Experimental fitting of the re-scaled Balje maps for low-Reynolds radial turbomachinery. *Energies*, vol. Volume 8, p. 7986-8000, ISSN: 1996-1073, DOI: 10.3390/en8087986

[11] Ishihama Y., Sakai K., Matsuzuki T., Hikone. Structural Analysis of Rotating Parts Of An Ultra Micro Gas Turbine. *Proc. Int. Gas Turbine Congress 2003* Tokio, November 2-7, 2003.

[12] Gaydamaka I. V., Efimov A. V., Ivanov M. Ja., Ivanov O. I., Nigmatullin R. Z., Ogarko N. I. Some Aerodynamic Performances of Small Size Compressor and Turbine Stages. *Proc. Int. Gas Turbine Congress* 2003 Tokyo.

[13] Capata R. Turbocharged Decoupling and Turbine Electrification Design for Mild-Hybrid Vehicle. *IMECE2021-68935. Proc. IMECE2021 congress*, November 1-5-USA

[14]] Matsuura K., Kato C., Yoshiki H., Matsuo E., Ikeda H., Nishimura K., Sapkota R. Prototyping Of Small-Sized Two Dimensional Radial Turbines *Proc. Int. Gas Turbine Congress* 2003 Tokio, November 2-7, 2003.

[15] Iwai. Thermodynamic Table For Performance Calculations In Gas Turbine Engine *Proc. Int. Gas Turbine Congress 2003* Tokio, November 2-7, 2003

[16] Capata R. Experimental tests of the operating conditions of a micro gas turbine device. *Journal of Energy and Power Engineering*, vol. 9, p. 326-335, ISSN: 1934-8975, doi: 10.17265/1934-8975/2015.04.002, 2015.

[17] Capata R., Sciubba E. Study, Development and Prototyping of a Novel Mild Hybrid Power Train for a City Car: Design of the Turbocharger. *Appl. Sci*. 2021, 11(1), 234; https://doi.org/10.3390/app11010234

[18] Ahmed A.; Soffker D. Towards Optimal Power Management of Hybrid Electric Vehicles in Real-Time: A Review on Methods, Challenges, and State-Of-The- Art Solutions. *Energies* 2018, 11, 476.

[19] Capata R.; Sciubba, E. The low emission Turbogas hybrid vehicle concept-preliminary simulation and vehicle packaging. *J. Energy Resour. Technol*. 2013, 135, 13.

[20] Capata, R.; Sciubba, E. The Lethe (Low Emissions Turbo-Hybrid Engine) city car of the University of Roma 1: Final proposed configuration. *Energy* 2013, 58, 178–184.

[21] Wei, Z.; Xu, J.; Halim, D. HEV power management control strategy for urban driving. *Appl. Energy* 2017, 194, 705–714. R.

[22] Mocera, F.; Martini, V.; Somà, A. Comparative Analysis of Hybrid Electric Architectures for Specialized Agricultural Tractors. Energies 2022, 15, 1944. https://doi.org/10.3390/en15051944

[23] Martellucci, L.; Capata, R. High Performance Hybrid Vehicle Concept—Preliminary Study and Vehicle Packaging. Energies 2022, 15, 4025. https://doi.org/10.3390/ en15114025

[24] Ehsani, M.; Singh, K.V.; Bansal, H.O.; Mehrjardi, R.T. State of the Art and Trends in Electric and Hybrid Electric Vehicles. Proc. IEEE 2021, 109, 967–984.

https://doi.org/10.52202/069564-0244

[25] Hu, X.; Liu, T.; Qi, X.; Barth, M. Reinforcement Learning for Hybrid and Plug-In Hybrid Electric Vehicle Energy Management: Recent Advances and Prospects. IEEE Ind. Electron. Mag. 2019, 13, 16–25.

[26] Nguyễn, B.-H.; Trovão, J.P.F.; German, R.; Bouscayrol, A. Real-Time Energy Management of Parallel Hybrid Electric Vehicles Using Linear Quadratic Regulation. Energies 2020, 13, 5538.

[27] Liu, T.; Tan, W.; Tang, X.; Zhang, J.; Xing, Y.; Cao, D. Driving conditions-driven energy management strategies for hybrid electric vehicles: A review. Renew. Sustain. Energy Rev. 2021, 151, 111521.

[28] Guo, N.; Zhang, X.; Zou, Y.; Guo, L.; Du, G. Real-time predictive energy management of plug-in hybrid electric vehicles for coordination of fuel economy and battery degradation. Energy 2020, 214, 119070.

[29] Xia, G.; Cao, L.; Bi, G. A review on battery thermal management in electric vehicle application. J. Power Sources 2017, 367, 90–105.

[30] Leibowitz, H.; Smith, I.K.; Stosic, N. Cost-Effective Small Scale ORC Systems for Power Recovery from Low-Grade Heat Sources. In Proceedings of the ASME 2006 International Mechanical Engineering Congress and Exposition, Chicago, IL, USA, 5–10 November 2006.

[31] Tocci, L.; Pal, T.; Pesmazoglou, I.; Franchetti, B. Small Scale Organic Rankine Cycle (ORC): A Techno-Economic Review. Energies 2017, 10, 413.

[32] ORC System. Available online: https://www.turboden.com/products/2463/orc-system (accessed on 20 January 2023).

[33] Li, L.; Tao, L.; Li, Q.; Hu, Y. Experimentally economic analysis of ORC power plant with low-temperature waste heat recovery. Int. J. Low-Carbon Technol. 2021, 16, 35–44.

[34] Jafari, A.; Yang, C.; Chang, C. Optimization of heat exchanger size of a 10 kW organic Rankine cycle system. Energy Procedia 2017, 129, 851–858.

[35] Unamba, C.K.; White, M.; Sapin, P.; Freeman, J.; Lecompte, S.; Oyewunmia, O.A.; Markidesa, C.N. Experimental Investigation of the Operating Point of a 1-kW ORC System. Energy Procedia 2017, 129, 875–882.

[36] Landellea, A.; Tauveron, N.; Revellin, R.; Haberschill, P.; Colasson, S. Experimental Investigation of a Transcritical Organic Rankine Cycle with Scroll Expander for Low-Temperature Waste Heat Recovery. Energy Procedia 2017, 129, 810–817.

[37] Capata, F. Pantano. Expander design procedures and selection criterion for small rated Organic Rankine Cycle systems *Energy Science & Engineering*, Volume8, Issue10, October 2020. DOI:https://doi.org/10.1002/ese3.710

[38] Dumont O, Talluri L, Fiaschi D, Manfrida G, Lemort V. Comparison of a scroll, a screw, a Roots, a piston expander and a Tesla turbine for small-scale organic Rankine cycle. *5th International Seminar on ORC Power Systems*, September 9–11, 2019, Athens, Greece.

[39] Oudkerk JF, Dickes R, Dumont O, Lemort V. Experimental performance of a piston expander in small-scale organic Rankine cycle. *Proc of Int. Conf. on Compressors and their Systems*; 2015.

[40] Seher D, Lengenfelder T, Gerhardt J, Eisenmenger N, Hackner, M, Krinn I. Waste Heat Recovery for Commercial Vehicles with a Rankine Process. *Proceeding of the 21st Aachen Colloq*; 2012.

[41] Bonafoni G., Capata R. Proposed Design Procedure of a Helical Coil Heat Exchanger for an Orc Energy Recovery System for Vehicular Application. *Mechanics, Materials Science & Engineering Journal*, 10.13140/RG.2.1.2503.5282

[42] Capata R., Zangrillo E. Preliminary design of compact condenser in an organic rankine cycle system for the low grade waste heat recovery. *Energies* 2014, 7(12), 8008-8035; https://doi.org/10.3390/en7128008

[43] Capata R., Piras G. Condenser Design for On-Board ORC Recovery System. *Appl. Sci*. 2021, 11(14), 6356; https://doi.org/10.3390/app11146356

[44] Kuppan, T. *Heat Exchanger Design Handbook*, 2nd ed.; CRC Press: New York, NY, USA, 2013.

https://doi.org/10.52202/069564-0244